ANALYSIS OF A DOUBLY-EXCITED BRUSHLESS RELUCTANCE MACHINE BY FINITE ELEMENT METHOD

Longya Xu
Member, IEEE

The Ohio State University
Department of Electrical Engineering
2015 Neil Avenue
Columbus, Ohio 43210

Abstract - This paper presents a magnetic field analysis of an original Doubly-Excited Brushless Reluctance Machine (DEBRM). The stator of the DEBRM consists of two sets windings with different pole numbers. The rotor is an axially laminated structure with a pole number different from either of the stator windings. The finite element method is applied by which the magnetic vector potentials under no-load and loaded conditions are solved. The pulsating airgap flux distribution is plotted and the mutual coupling of the dual stator windings is derived based on the field solutions. The electromagnetic torque capability of the DEBRM is evaluated and compared with that of the equivalent induction machine.

Introduction

Reluctance machines have been actively researched over the past two decades, and very promising results have been obtained. It has been found that many types of reluctance machines are attractive alternatives to the more conventional PM synchronous and induction machines in converter-fed adjustable speed drive applications [1,2,3]. The fundamental features of the reluctance machine include its simple and rugged structure, very good compatibility with the power electronic converters, and improved overall performance over a wide torque-speed range [4].

The more recent investigation has revealed that the Doubly-Excited Brushless Reluctance Machine (DEBRM) is another potential candidate in converter-fed variable speed drive and generating systems [5]. The DEBRM can be constructed in such a version that while it emulates the performance of a doubly-fed induction machine in a slip-power recovery variable system, it eliminates the complicated slip-rings and brushes. The advantages of a slip-power recovery variable speed system such as reduced power converter rating and cost, super- and sub-synchronous speed operation capability, and flexible active and reactive power control are retained by the DEBRM [4,5].

The DEBRM employs two separate windings on the stator of different pole numbers. The rotor is equipped with axially laminated reluctance segments with pole number different from either of the stator windings. In operation, the reluctance rotor modulates the stator MMFs and produces complicated pulsating airgap flux. It is seen that the operation principle of DEBRM is much less straight forward than that of a conventional induction or synchronous machine.

The linear model of the DEBRM has been studied by applying the winding function theory and the extended d-q transformation [5]. However, the results of a nonlinear model of such a machine described directly in the A-B-C phase system have never been published. In this paper, a detailed nonlinear analysis of the DEBRM machine in the A-B-C phase system is presented by using the finite element method. First, the magnetic field is calculated strictly according to the geometry and the winding connections of the machine, and the magnetic nonlinearity is included by incorporating the B-H curve into calculation. Secondly, various flux patterns throughout the cross-section of the machine are plotted. The winding flux linkages are calculated based on the solution of the magnetic vector potentials. The mutual coupling between the two sets of stator windings is derived. Thirdly, the load condition is simulated and the performance is evaluated. Without any reference frame transformation, the finite element analysis presented in this paper directly plots the magnetic field in detail and highlights the mutual coupling between the dual sets of stator winding under various no-load and loaded conditions. The internal magnetic field analysis is translated into the terminal characteristics of the machine. Hence, the analysis presented in this paper provides insights into the optimal design and control of a practical DEBRM.

0-7803-0634-1/92$03.00 ©IEEE

DEBRM Geometry and Winding Structure

The DEBRM machine assembly is shown in Figure 1. The major dimensions and the detailed specifications of the DEBRM are given in Table 1. The stator has two sets of three phase quasi-sinusoidally distributed windings. The pole number of one stator winding is p =2 and another q = 4 (referred as 2-pole and 4-pole windings later on). The spatial distribution of the dual windings is described in Figure 2. When the 2-pole and 4-pole windings are

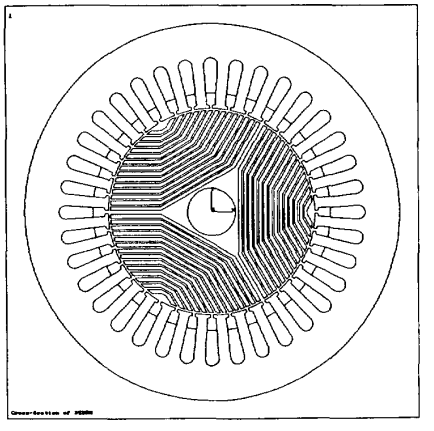

Figure 1 DEBRM Stator and Rotor Assembly

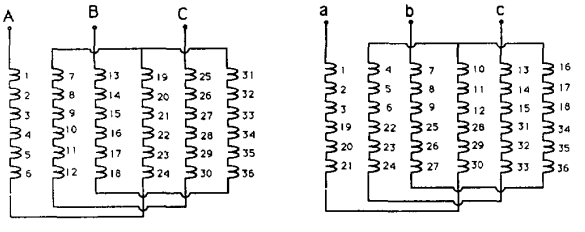

2-pole Winding Distribution 4-pole Winding Distribution

Figure 2 Dual Stator Windings of the DEBRM

doubly excited by two sinusoidal currents at frequencies of ω_1 and ω_2, two rotating MMFs *(not flux)* along the airgap at speed of ω_{1m} and ω_{2m} are generated, where

$$\omega_{1m} = \frac{2\omega_1}{p} \tag{1}$$

and

$$\omega_{2m} = \frac{2\omega_2}{q} \tag{2}$$

The rotor consists of 3 pieces of axially laminated segments and the laminations in each segment are interleaved with non-magnetic material as indicated in the figure. Whenever the magnetic flux lines are forced to travel in a path normal to the lamination plane, the flux lines encounter the maximum reluctance. Yet, whenever the flux lines are driven to travel along the lamination plane, the reluctance is minimum.

In addition to the features described above, the structure of the DEBRM analyzed in this paper differs from the previous ones in [4,5] in two aspects:

1) The number of rotor segments is 3, an odd number. Consistent with the rotor segment number, the pole numbers for the two stator windings are reduced to 2 and 4, the smallest numbers allowable. In this way, the machine can reach the highest speed for a given frequency. This paper will address the effects of an odd number of rotor segments.

2) The number of slots per phase per pole is relatively large. For the 4-pole stator winding, this number is 3 and for the 2-pole winding it is 6. It has been discussed in [4] that the harmonics of the winding distribution affect the current waveform significantly in a DEBRM. By selecting the number of slots per pole per phase to be large, the winding distribution harmonics are reduced. Using the finite element method, this paper will discuss the harmonic improvement.

As discussed in [4,5], the DEBRM must follow the frequency constraint to produce useful average torque. Assuming that the frequencies of the voltages supplied to 2-pole and 4-pole windings are ω_1 and ω_2 respectively, the rotor speed is governed by the equation:

$$\omega_{mr} = \frac{\omega_1 \pm \omega_2}{(p+q)/2} \tag{3}$$

where ω_{mr} is the mechanical speed of the rotor. Although the MMFs created by each individual set of stator winding are smooth rotating sine waves along the airgap, the combined MMF will be pulsating in nature since the two MMF vectors rotate at different angular velocities. In addition, the pole number of the rotor is neither of those of the stator MMFs. Consequently, the combined MMF is modulated by the rotor permeance, resulting in a complicated airgap flux pattern.

In this paper, Eq. (3) will be used as a guideline to choose the excitation current frequency and the rotor speed. However, the equation does not function as an assumption that the conclusions are drawn based upon.

Field Analysis by the Finite Element Method

In order to analyze the magnetic field of the DEBRM and relate the terminal characteristics to the complicated airgap flux pattern, the finite element method is chosen to solve for the magnetic field [6]. Assuming a magnetic vector potential, A_z, in the z-direction, the magnetic field of the DEBRM is described by the Poisson Equation:

$$\frac{\partial}{\partial x}\left(\gamma \frac{\partial A_z}{\partial x}\right) + \frac{\partial}{\partial y}\left(\gamma \frac{\partial A_z}{\partial y}\right) = -J_o \tag{4}$$

where γ is the magnetic reluctivity and J_o is the excitation current density. In the field analysis, γ is determined by the nonlinear B-H curve and J_o is determined from the excitation current. Additional assumptions are made: i) the machine is relatively long and the field quantities are invariant in the z-direction; ii) the iron material is not grain-oriented and the B-H curve is single-valued; and iii) the flux lines are confined within the stator core.

The machine model is discretized into approximately 4000 elements as shown in Figure 3. To guarantee computation accuracy, the elements in the neighborhood of the airgap are dense. An enlargement of the discretized airgap is shown in the same figure.

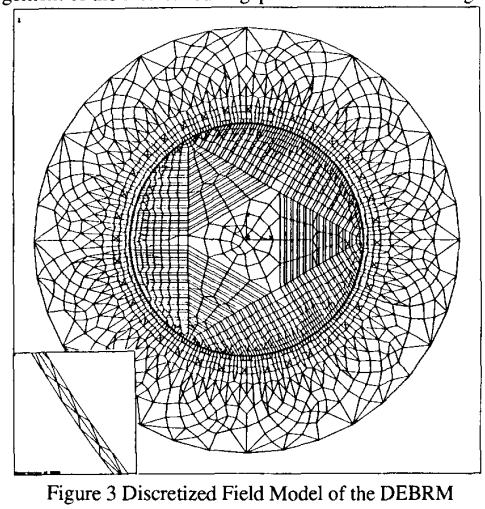

Figure 3 Discretized Field Model of the DEBRM

No-Load Operation

The no-load operation of the DEBRM is defined as the same as that for any other type of electric machines: *no electromechanical energy conversion occurs* when the rotor rotates. It will be made clear that for the DEBRM this corresponds to the case of exciting only one of the two stator windings. In order to simulate the mechanical rotation of the rotor, a constant rotor speed is assumed. The incremental angle of rotor rotation is chosen to be a slot pitch, 10 degrees mechanical for computation convenience.

1) Airgap Flux Distribution

The no-load operation of the DEBRM can be simply shown when the 2-pole or 4-pole winding is excited with a three phase current at zero frequency (DC). In this way, a stationary, sinusoidally distributed MMF is created. With the rotor permeance provided by the 3 axially laminated segments, a non sinusoidal airgap flux is produced. The non-sinusoidal airgap flux distribution is shown in Figure 4 at 6 different rotor positions spanning 120 degree rotation. In the figure, the 2-pole winding is excited with DC current, and the rotor advances in a 20° step for every plot. It is interesting to observe that no explicit number of poles or traveling flux wave can be identified from all of the plots. This seemed a logic result of the different pole numbers of the MMF and the rotor segments It is also noticeable that for each rotor position, the peak airgap flux changes to a different value at a different location.

Another important observation of the no-load flux distribution is its asymmetry over the machine cross-section. The unsymmetry of the flux distribution can be easily identified by drawing a vertical line through the center of the DEBRM as shown in Figure 5. It is evident that the flux density on the LHS is higher than that on the RHS. The asymmetrical flux distribution is believed to be the result of the odd-number segments of the rotor.

Since the three rotor segments are identical, the flux repeats the distribution pattern for every 120° rotor rotation. However, if the excitation frequency is not zero, or equivalently, the MMF wave

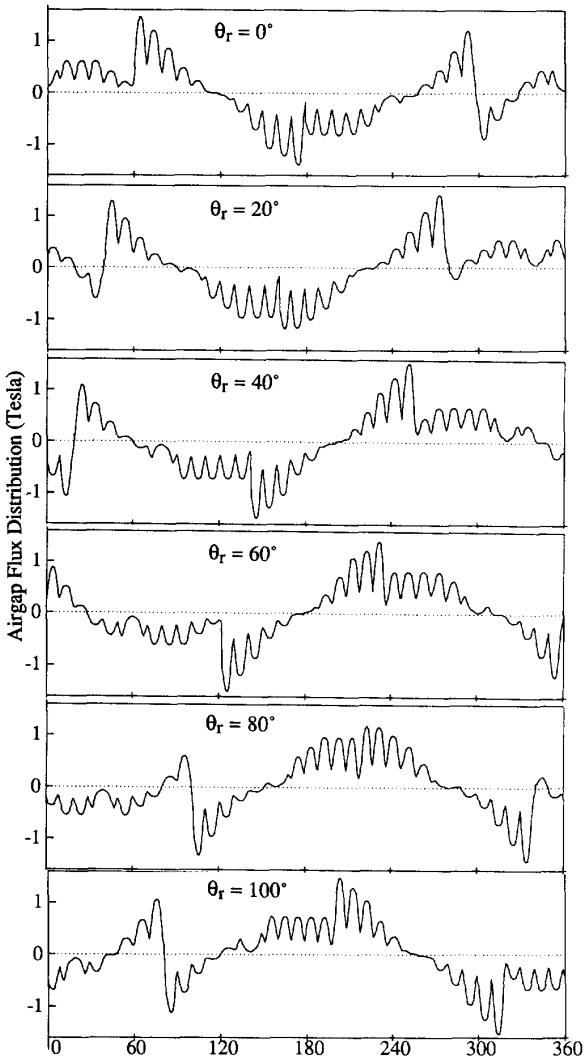

Figure 4 No-Load Airgap Flux Distribution at 6 Rotor Positions

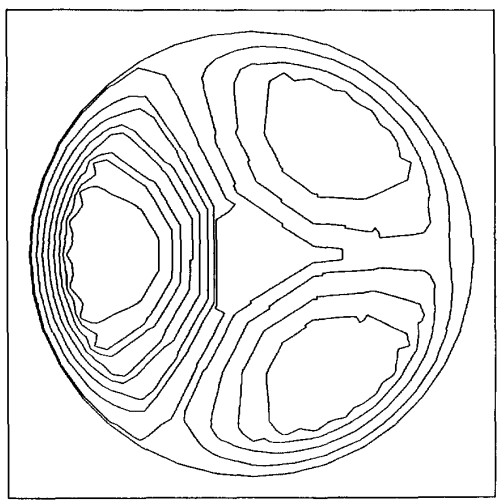

Figure 5 Flux Distribution over the Cross-Section at No-Load

starts to rotate, then the flux pattern repetition becomes more complicated. In general, the flux repetition is solely dependent on the relative position of the rotor segments and the MMF. For example, the flux distribution will repeat its pattern for every 120° increment of the relative displacement between the rotor and the MMF. In such a situation, it is not essential to emphasize whether the relative displacement is created by the rotor movement, the MMF wave movement, or both. Therefore, the airgap flux distribution shown in Figure 4 is still representative for the 2-pole winding excitation of any frequency at any rotor speed. For the 4-pole winding excitation alone, the airgap flux pattern is different. However, the features shown in 2-pole winding excitation, such as the nonsinusoidal distribution, the variable peak flux, and the non-identifiable pole number remain.

Given such a non-sinusoidal, pulsating airgap flux distribution, we immediately face a difficulty in revealing the much less straight forward mechanism of electromechanical energy conversion embedded in the DEBRM. Plausibly, one might resort to the harmonic decomposition method that takes the fundamental component into account while neglecting the nonessential harmonics. However, the complicity even exists in the DEBRM that what is the "fundamental component" and what are those "negligible harmonics". As a matter of fact, it will be made clear in this paper that harmonic decomposition is not a relevant approach for the DEBRM analysis.

2) Winding Flux Linkage

Winding flux linkage, obtained by looking into the winding through its terminals, provides a convenient means to investigate the electromechanical energy conversion of an electric machine. In particular, if the flux linkage of the stator winding changes as a function of the rotor movement, a speed voltage will be induced and electromechanical energy conversion becomes realizable. To verify the energy conversion principle of the DEBRM, the flux linkage of the stator windings have been investigated through finite element analysis.

Consider a single turn coil in a 2-D magnetic field described by the vector potential, A_z, as shown in Figure 6. The flux linkage of the single-turn coil may be evaluated from the magnetic vector potential A_z as:

$$\lambda_{coil} = L \int_{a_1}^{a_2} B \, d\ell$$

$$= L \int_{a_1}^{a_2} \frac{\partial A}{\partial \ell} d\ell = A_z(a_1) - A_z(a_2) \qquad (5)$$

where $A_z(a_1)$ and $A_z(a_2)$ are the vector potentials at the locations of the coil two sides, a_1 and a_2. L is the effective length of the coil experiencing the flux variation. If the coil has N turns at the same

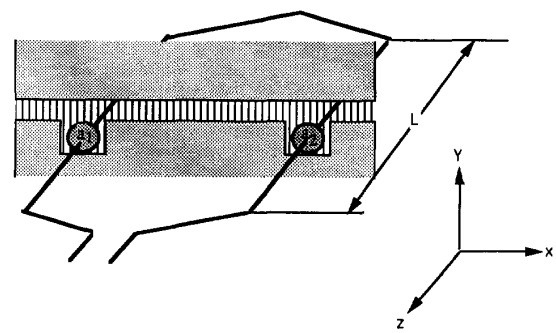

Figure 6 Coil Flux Linkage Evaluation from Vector Potentials

location, the flux linkage will be N times as large. Further, if a winding is formed by several coils connected in series at different locations, the total flux linkage of this winding will be the sum of the flux linkage associated with each individual coil. This method of calculating winding flux linkage from the solution of the vector potential is applied in the paper.

As an example of calculating the winding flux linkage from the vector potentials, the location and polarity of the Phase A winding of 4-poles is shown in Figure 7. This winding is wound into two layers and divided into four groups. It is easy to prove that the total flux linkage of this winding equals to the sum of the vector potentials at the locations marked by "+" sign minus the sum of the vector potentials at the locations marked by "-" sign. It is clear that the saturation is included automatically, and individual self and mutual inductance calculations are avoided by this method.

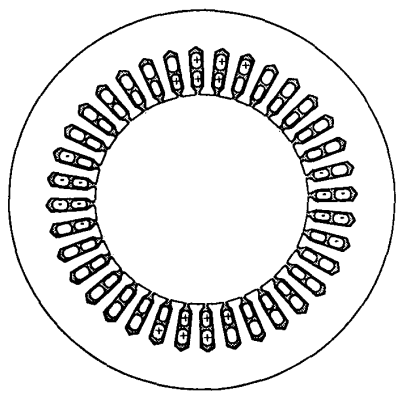

Figure 7 Spatial Distribution of One Phase 4-Pole Winding

In a similar manner, all of the flux linkages of the other windings can be calculated. To relate the magnetic field analysis to the terminal characteristics of the DEBRM, two types of winding flux linkage of the DEBRM are particularly concerned. The first type is called *the self flux linkage* defined as: the flux linked by one phase of the winding when the three phase windings with the same pole number are excited by a three phase symmetric current. This so-defined self flux linkage can be visualized in an alternative way. That is, if an airgap flux is created by three phase windings in a set, the self flux linkage is the result of how the flux is weighted by this phase winding distribution. Note that since the flux linkage is weighted by the winding, the self linkage will not only related to the flux distribution but also to the winding distribution. Since the winding flux linkage is a terminal quantity, it is also considered an integrated description of the magnetic flux from the an individual winding point of view .

The second type is called *the mutual flux linkage* defined as: the flux linked by one of the other three phase winding with a different pole number when the three phase windings are excited by a three phase symmetric current. Similarly, the mutual flux linkage can be interpreted as the result of how the same flux generated as previously is felt or weighted by one phase winding of another set with a different pole number. It can be predicted that since the pole pitches, or pole pitches of the two set windings are different, the "feelings" of the windings towards the same flux will be substantially different.

Based on the vector potential solution, several important results of the flux linkage calculation are shown in Figure 8. In Figure 8(a), the self flux linkage of the 2-pole winding is plotted versus the rotor positions. Although the airgap flux is not sinusoidally distributed in space as plotted previously, the flux linkage obtained by looking into the terminals of the winding possesses a very smooth and regular pattern. When the excitation is

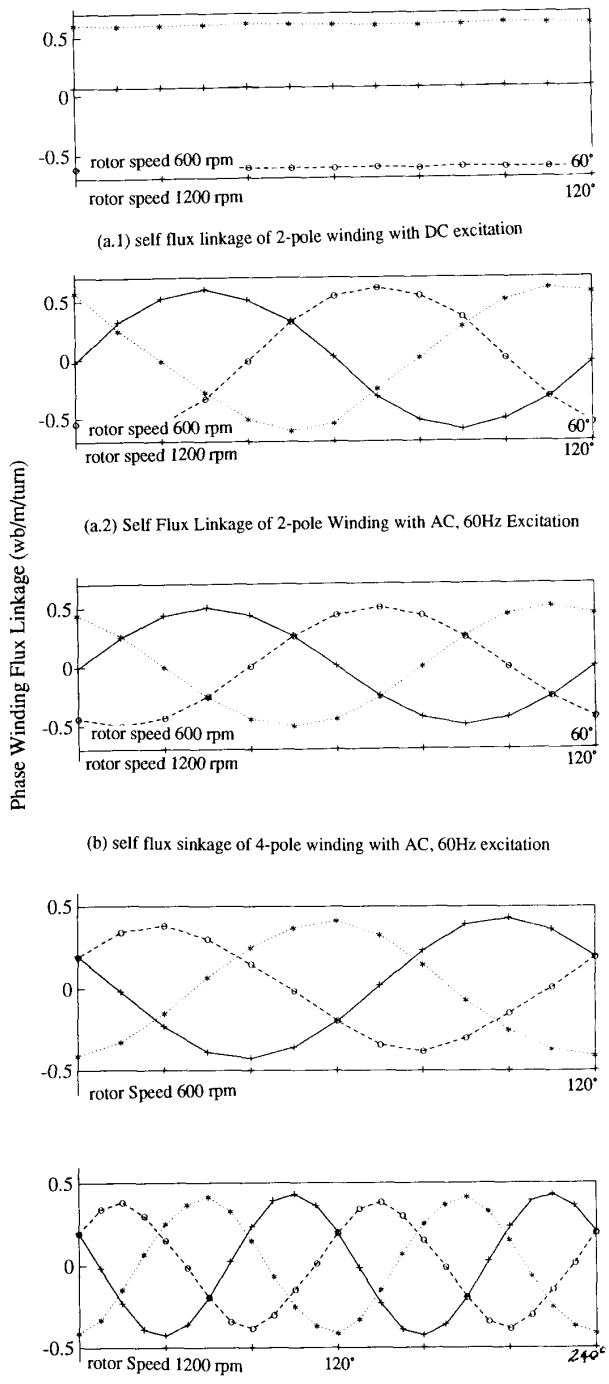

(a.1) self flux linkage of 2-pole winding with DC excitation

(a.2) Self Flux Linkage of 2-pole Winding with AC, 60Hz Excitation

(b) self flux sinkage of 4-pole winding with AC, 60Hz excitation

(c) mutual flux linkage of 4-pole winding with DC excitation of 2-pole winding

Figure 8 Self and Mutual Flux Linkages versus Rotor Positions

DC, the flux linkage of the winding is also DC regardless of the rotor speed and position. When the excitation changes to AC, for example 60 Hz, the self flux linkage changes correspondingly to 60 Hz regardless of the rotor speed and position. The self flux linkages of the three phase windings in the same winding set have a 120° phase angle difference.

In Figure 8(b), the self flux linkage of the 4-pole winding is shown. Similar characteristics can be observed. The self flux linkage of the 4-pole winding is not a function of the rotor position. Instead, the flux linkage changes periodically at a frequency corresponding to that of the excitation current.

By contrast, the mutual flux linkage behaves very differently. In Figure 8(c), the mutual flux linkage of the 4-pole winding is plotted. In this case, the 2-pole winding is excited by the three phase current at zero frequency, and the vector potential associated with the 4-pole winding is calculated. It can be observed that the mutual flux linkage is closely related to the rotor position. In effect, the frequency relation constrained by Equation (3) is verifiable by the figure. The dependence of the mutual flux linkage variation can also be verified by computing the mutual flux linkage of the 2-pole winding while exciting the 4-pole winding. The computation results show the same results as those in the other case.

Note that, in the flux linkage computation, we have used the complete solution of the field analysis and exact winding connection. Equivalently, the magnetic non-linearity and all of the space harmonics of the flux are included in the computation. Therefore, it may be contended that if we had neglected some of the flux harmonics, the results on the flux linkage calculation would be very different. Summarizing the flux linkage calculation, we can make the following very important conclusions regarding the DEBRM :

a) The self flux linkage is independent of the rotor position. The frequency of the self flux variation is the same as that of the excitation current.
b) The mutual flux linkage is rotor position dependent. The variation of the mutual flux linkage is a sinusoidal function of the rotor position and the frequency of the function follows the constraint given by Eq. (3).

c) The computation of the winding self and mutual flux linkages is based on the complete solution of the field, and all of the space harmonics of the airgap flux distribution are included.

3) Induced No-Load Speed Voltage

By definition, the induced speed voltage is simply the derivative of the flux linkage. Up to this point, we know that if only one set winding is excited, for example, the 2-pole winding, the self flux linkage of the 2-pole winding will not be affected by the rotor movement. Therefore, it is impossible to induce speed voltage in the 2-pole winding so as to realize electromechanical energy conversion. This can also be understood from the fact that the rate of electromechanical energy conversion is expressed as the product of the current by the speed voltage.

Nevertheless, the magnetic flux established by the 2-pole winding will be linked by the 4-pole winding as the mutual flux linkage. More significantly, this mutual flux linkage is affected by the movement of the reluctance rotor. Therefore, the speed voltage is induced in the 4-pole winding as the reluctance rotor rotates. As the result of the mutual flux linkage variation, the induced speed voltage is sinusoidal.

For the similar reason, the excitation of the 4-pole winding will not generate speed voltage in the winding itself but will generate speed voltage in the 2-pole winding when the rotor rotates. Since the variation of the mutual flux linkage is rotor speed dependent, the frequency of the induced speed voltage is also determined by the rotor speed.

Loaded Operation

1) Principle of Torque Production

It has been made apparent in the preceding analysis that in the DEBRM the mutual flux linkage of the windings varies sinusoidally with respect to the rotor position. If a current with the same frequency as that of the mutual flux linkage variation is injected into the winding, an electromagnetic torque will be produced. The torque can be expressed as:

$$T_e = \frac{3\,E_p\,I_p\cos\phi + 3\,E_q\,I_q\cos\phi}{\omega_{rm}}$$

$$= \frac{3\omega_1\lambda_{mq}\,I_p\sin\phi + 3\omega_2\lambda_{mp}I_q\sin\phi}{\omega_{rm}}$$

$$= \frac{3}{2}(p+q)\,\lambda_{mq}\,I_p\sin\phi \qquad (6)$$

where the E_p and E_q are the induced speed voltages due to the mutual flux linkages; I_p and I_q are the injected phase currents in the dual stator windings; ϕ is the angle between the induced speed voltage and the current; λ_{mp} and λ_{mq} are the mutual flux linkages under the given currents. Note that in the torque derivation, the relation $\lambda_{mp}/\lambda_{mq} = I_p/I_q$ is used and the frequency constraint given in Equation (3) is observed.

The loaded operation of the DEBRM is simulated according to the principle implied by Equation (6). In particular, the three phase current is injected in phase with respect to the induced speed voltage of the winding, or equivalently, orthogonal to the mutual flux linkage component. Because the induced speed voltage and injected current are in phase, the maximum torque production for the given currents is expected. The orthogonal current injection with respect to the mutual flux linkage is actually the field orientation control similar to that in a synchronous machine operation. Note that the current injection is oriented to the mutual flux linkage variation which, in turn, is the function of the rotor position. Therefore, the current injection implementation can be realised by feeding back the signal of rotor positions.

Furthermore, as indicated by Equation (6), the torque production of the machine is the product of the flux linkage by the current, independent of the rotor speed. Therefore, it may be said that the torque capability of the DEBRM can be evaluated at one particular rotor speed. In the following evaluation, the rotor speed is chosen at 1200 rpm.

2) Evaluation of Torque Capability

The in-phase current injection with respect to the induced speed voltage is implemented in two steps in the finite element analysis. In the first step, the no-load vector potential is calculated with the excitation current placed in the 2-pole winding. Following the calculation of the vector potential, the mutual flux linkage of the 4-pole winding is obtained and the phase angle of the mutual flux linkage with respect to the rotor position is located. In the second step, the three phase current is injected to the 4-pole winding, orthogonal to the mutual flux linkage variation and, thus, in phase with the induced speed voltage. With both 2-pole and 4-pole windings doubly excited, the vector potential and the total flux linkage of the winding are recalculated.

The torque capability of the DEBRM is calculated by the two step approach and compared with an equivalent induction machine. As indicated in Table 1, the main dimensions of the DEBRM are identical to that of the induction machine rated at 7.5 hp with the synchronous speed of 1800 rpm. The stator slot number and size are also the same as those of the induction machine. The major difference is that a current free, reluctance rotor is used in the DEBRM, while a short-circuit, cage rotor is used in the induction machine.

Using the rated current of the induction machine as the base current, torque production of the DEBRM is evaluated at three current levels. The resultant phase flux linkage variation and the current of the 4-pole winding are plotted versus the rotor position in Figure 9. It can be seen that the flux linkage of the winding is no longer orthogonal to the current. Be mindful that when the DEBRM is doubly excited, the magnetic vector potentials are determined by the currents in both sets of the stator windings and so is the flux linkage. Therefore, the flux linkage of the winding contains not only the mutual flux component but also the self flux component resulting in the phase angle and magnitude variation as shown in the figure.

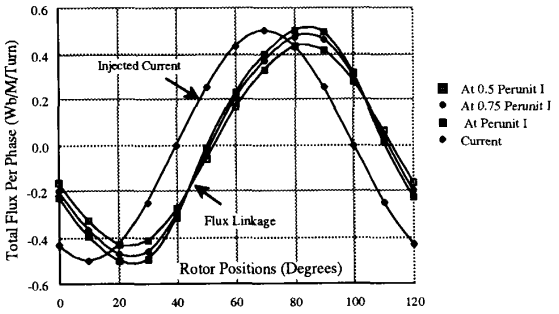

Figure 9 Phase Angle Between the Current and the Total Flux

Figure 10 (a) and (b) show the flux distribution over the cross-section of the DEBRM for both no-load and loaded conditions at one rotor position. In the no-load condition, the relatively smooth flux lines form three curls and each of the curls is almost symmetric about its axis. In terms of torque production based on the Maxwell stress principle, the smooth flux lines and the symmetry of the curls indicate an equilibrium state and zero torque production. However, the flux lines in the loaded condition are much denser and less smoother than those in the no-load condition, particularly in the rotor lamination part. The asymmetry of the curls formed by the flux lines in loaded condition is evident, indicating torque capability of the DEBRM. Direct calculation of the torque production from the flux lines is possible but will be very complicated and less accurate.[7,8]

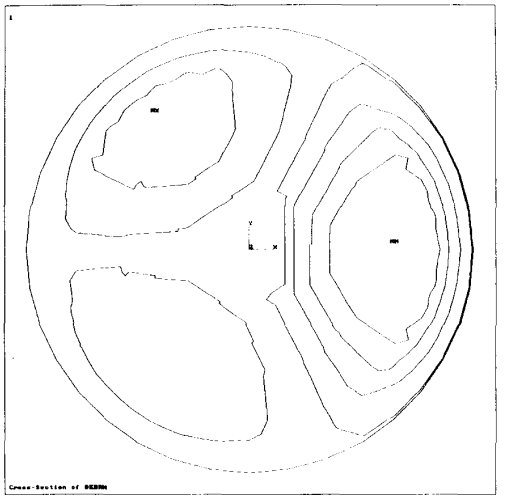

(a) Flux Distribution in No-Load Condition

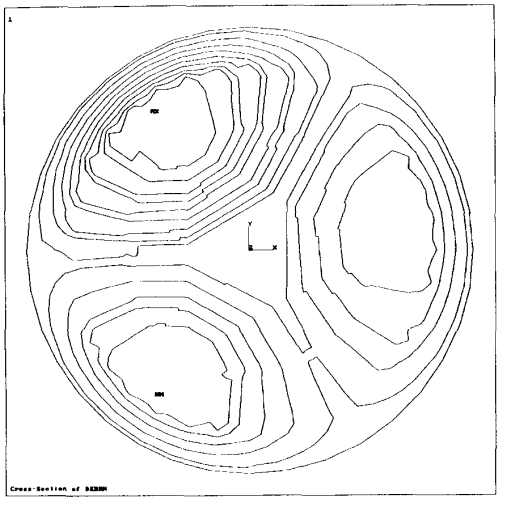

(b) Flux Distribution in Loaded Condition

Figure 10 Comparison of Flux Distribution

Using the calculated flux linkage of the winding shown in Figure 9 the torque production of the DEBRM is evaluated according to the equation:

$$T_e = \frac{3\ V_p\ I_p \cos\theta}{\omega_{rm}}$$

$$= \frac{3}{2}(p+q)\ \lambda_p\ I_p \sin\theta \qquad (7)$$

where the V_p and I_q are the phase voltate and current; θ is the angle between the phase voltage and the current; λ_p is the total flux linkage including the mutual and self flux linkage components. The torque capability of the DEBRM is shown in Figure 11. For the rated current the torque capability of the equivalent induction machine from the experiment is shown in the same figure. It is noticeable that at the rated current level, the torque production of the DEBRM is actually higher than that obtainable by the induction machine. However, the conductor area in the DEBRM is reduced to the half of that in the induction machine and, thus, the conduciton losses will increse proportionally. From the comparison, it appears that the torque capability of the DEBRM has not outperformed its induction machine counterpart. Neverthelss, the higher torque capability has already demonstrated the DEBRM potential. We may consider the fact that the geometry of the DEBRM presented is based on its induction machine counterpart for comparison, not optimally designed. It can be contended that with an optimal design, improved performance of the DEBRM can be expected.

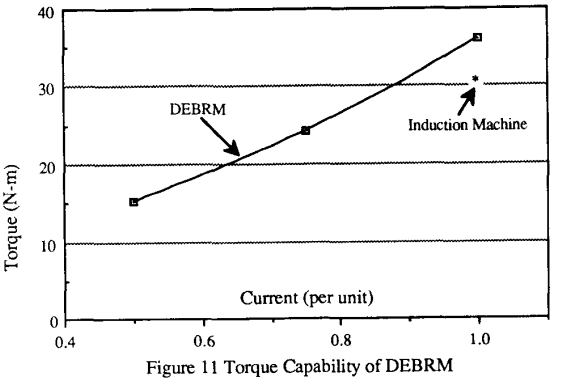

Figure 11 Torque Capability of DEBRM

3) Saturation Effect

The saturation effect of the DEBRM on the torque production is investigated by the finite element analysis. In the unsaturated case, the torque production of the DEBRM is evaluated from Equation (6) which states that the torque is the cross product of the mutual flux linkage by the current vector. However, as soon as the torque current vector is injected, the MMF generating the mutual flux will be superimposed by the MMF generating the self flux. As a result, the total MMF generates a compound flux which determines the phase voltage and the torque production.

If the DEBRM is not saturable (linear), the compound flux will be directly proportional to the total MMF, and the torque evaluated from Equation (6) will not be altered. However, in the saturated situation the compound flux will not be directly proportional to the total MMF and the torque production must be evaluated from Equation (7). The torque production of the DEBRM based on Equations (6) and (7) at the same current levels are evaluated and plotted in Figure 12. It is seen that a 15-18% drop of the torque production can be observed.

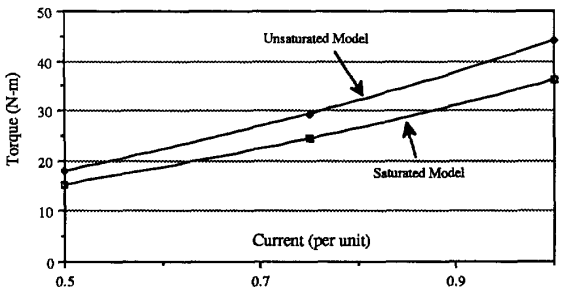

Figure 12 Saturation Effect on Torque Production

Conclusions

The complicated flux distribution inside the DEBRM, coupled with the magnetic nonlinearity, and the less straight forward terminal characteristics of the DEBRM have been investigated in detail by the finite element method. The following conclusions have been reached by the analysis:

1) The airgap flux distribution of the DEBRM is non sinusoidal. However, the non-sinusoidal airgap flux can not be treated by neglecting the harmonics as usual. Rather, from an integral point of view, the winding flux linkage evaluation is shown suitable to relating the nonsine flux distribution to the machine terminal characteristics. The terminal characteristics of the DEBRM derived by flux linkage evaluation are shown to have a sine nature.

2) The self flux linkage of the stator winding is independent of the rotor position, similar to the magnetizing flux in an induction machine or the armature reaction flux in a round-rotor synchronous machine.

3) It is the mutual flux linkage variation interacted with the phase current in the DEBRM that accomplishes the electromagnetic torque production and electromechanical energy conversion.

4) The torque capability of the DEBRM is comparable to that of the equivalent induction machine. Further optimal design of the magnetic circuit of the DEBRM is possible to improve the performance.

5) Saturation effects of the DEBRM reduce the torque production by 15-18% compared with the unsaturated model.

In spite of the fact that the DEBRM is characterized by an airgap flux of pulsating amplitude, the paper also showed that field orientation control is an applicable concept to the DEBRM to enhance torque production. However, the field orientation may not be interpreted as the current vector oriented to the airgap flux vector as has been done in the conventional rotating flux electrical machines. A prototype is planned for experimental evaluation and the results will presented when they are ready.

Acknowledgment

The work presented in this paper is supported by a Research Initiation Grant ESC-9111256 from National Science Foundation. Assistance from Mr. N. Bai in computing the results is gratefully acknowledged.

References:

[1] M. R. Harris, J. W. Finch, J. A. Mallick, T. J. Miller, "A Review of the Integral Horsepower Switched Reluctance Drive", IEEE Trans. IAS, Vol. IA-22, July/Aug. 1986, pp. 716-721

[2] L. Xu and T. A. Lipo, "Analysis of a Variable Speed Singly-Salient Reluctance Motor Utilizing Only Two Transistor Switches," IEEE Trans. IAS, Vol. 26, no 2,-236, March/ April 1990.

[3] T. J. Miller, C. Costar, and Button, "Design of a Synchronous Reluctance Motor Drive," IEEE IAS Annual Meeting, October 5, pp 122-128.

[4] F. Liang, L. Xu, and T. A. Lipo, "Transient Model of the Doubly Fed Reluctance Motor", IEEE Transaction on Energy Conversion, Vol. 6, No. 1, March 1991, pp. 126-133.

[5] L. Xu, F. Liang and T. A. Lipo, "Analysis of a New Variable Speed Doubly Excited Reluctance Motor", Electric Machines and Power Systems, Vol. 19. No. 2, March 1991, pp. 125-138.

[6] P. P. Silver and R. L. Ferrari, "Finite Elements for Electrical Engineering" (book), Cambridge University Press, Cambridge, 1983.

[7] J. Penman and M. D. Grieve, "Efficient Calculation of Force in Electromagnetic Devices" IEE Proceedings, Vol. 133 Pt. B, No. 4, July 1986, pp. 212-216

[8] L. Xu, "Design and Evaluation of a Reluctance Machine Drive System", Ph. D. Dissertation, University of Wisconsin-Madison, 1990

Table 1

Specifications of the DEBRM

Ratings
Power rating: 5.0 hp
Synchronous Speed: 1200 rpm
Rated Voltage: 160 volts
Rated Current in Primary: 10 amps
Rated Current in Secondary: 10 amps

The main dimensions of the DEBRM are identical to those of the equivalent induction machine as listed in the following:

Ratings
Power rating: 7.5 hp
Rated Speed: 1750 rpm
Rated Voltage: 230 volts
Rated Current: 10 amps
Power Factor at Rated Load: 0.8

Main Dimensions
Stator Lamination OD: 9.001 in
Stator Lamination ID: 4.954 in
Effective Length of Stator Stack: 4.00 in